Robotica (2002) volume 20, pp. 637–651. © 2002 Cambridge University Press
DOI: 10.1017/S02635747002004435 Printed in the United Kingdom

A singularly perturbed method for pole assignment control of a flexible manipulator

Atsushi Konno,* Liu Deman† and Masaru Uchiyama*

(Received in Final Form: June 28, 2002)

SUMMARY

This paper focuses on using a singularly perturbed approach to derive a vibration damping control law in which a pole assignment feedback method is utilized. The composite control system is characterized by two components which can be computed separately. The one is Cartesian-based PI control which drives the end-effector of a flexible manipulator to track the desired time-based trajectory. The other is pole assignment feedback control which damps out vibrations during and at the end of trajectory tracking. An advantage of this composite control method in real implementation is that it does not require a derivative of the end-effector's position, and the derivatives of signals from the strain gauges. From the characteristics and implementation points of view, it appears to be simple to use. Laboratory experiments were conducted to evaluate the performance of the proposed control method.

KEYWORDS: Cartesian space; Flexible manipulator; PI control; Two time-scale; Pole assignment.

1. INTRODUCTION

Over the past two decades, there has been a great deal of work done on the modeling and control of flexible link manipulators. In 1975, Book et al. studied the feedback control problem of a two-link flexible robot arm.[1] Since then, theoretical and experimental research results have been reported extensively, e.g. optimal control,[2] adaptive control,[3] computed acceleration control,[4] sliding mode control,[5] robust control,[6] input preshaping control,[7–9] and neural network control.[10] The singular perturbation approach has attracted widespread attention.[11–14] Actually, there are too many published papers to be listed here. However, Most of the works mentioned above are mainly focused on the joint based control schemes and only a few works that involve the direct Cartesian space methods can be found.[15–17]

The motivation for using a Cartesian-based control strategy was inspired by flexible link deflections, because flexible link deflections can strongly effect the location and tracking accuracy of manipulators. In the Cartesian space trajectory control, most researchers generate trajectory planning by solving inverse kinematics accurately.[18–19] A compensating control technique for the quasi-static motion has been proposed,[20] and the compensability has been analyzed.[21] In a similar way, a feedforward multi-stage control scheme was suggested.[22] Their idea was first to compensate for the elastic deviation of the manipulator's end-effector and then control the end-effector's vibrations. Xi and Fenton developed a one-step numerical method for solving point-point quasi-static motion planning.[18] Dai et al. proposed a numerical iterative learning approach to solve the inverse kinematics effectively.[19] Although it is possible to obtain joint angle data required for tracking a specific trajectory preplanned in the Cartesian space, the trajectory generation procedure becomes tedious, since joint angles would have to be recalculated whenever the tracking trajectory changes. King et al. developed the pseudolink concept for representing the tip position of a flexible link.[23] The advantage of using the pseudolink approach is that trajectory planning may be carried out *a priori* under a rigid link assumption; the main drawback is that the pseudolinks would become longer or shorter when the joint configuration changes along the trajectory. In order to reduce the big computation burden for solving inverse kinematics, especially for flexible manipulators, and avoid significant position errors that occur in the end-effector due to incomplete kinematic compensation, this paper proposes a PI Cartesian-based control method as a gross motion control which drives the end-effector of a flexible manipulator to follow the planned trajectory.

Currently, the two-time scale approach has attracted much research effort. Using the approach, the dynamics of a flexible manipulator can be decomposed into two subsystems, namely, a slow subsystem and a fast subsystem. The slow subsystem corresponds to the rigid body movement, and the fast subsystem is mainly to account for the elastic modes. Usually, the composite control schemes are designed to deal with this kind of formulation. In this approach, the larger the stiffness of links, the more accurately the full-order system is approximated. The singular perturbation trajectory control method,[11–14] belong to this two-time scale control strategy. It is noteworthy from a practical viewpoint that it may not always be possible to separate the rigid motion from the elastic motion. This depends on the location of the first vibration mode and the bandwidth required in the slow rigid motion design. In order to improve the performance of a singular perturbation approach, the concept of *integral manifold* is utilized to represent the dynamics of the slow subsystem.[24]

* Dept. of Aeronautics and Space Engineering, Tohoku University, Aoba-yama 01, Sendai 980–8579 (Japan). E-mail: {konno, uchiyama}@space.mech.tohoku.ac.jp
† Dept. of Automatic Control, Northeastern University, ShenYang City, LiaoNing Province (People's Republic of China). E-mail: dmliu@ramm.neu.edu.cn

https://doi.org/10.1017/S0263574702004435 Published online by Cambridge University Press

It is reasonable to assume that a flexible manipulator would be easier to control if the vibrations could be neglected, and only the rigid terms were significant. Thus, there is motivation to pursue schemes which combine a feedback controller to eliminate vibrations for end-effector position control. An efficient method for multivariable digital control of a flexible manipulator based on pole assignment by state feedback is proposed so that vibrations are eliminated as soon as possible in the process and at the end of trajectory tracking. The concept of coordinating the motion of a robot arm based on multivariable pole assignment by state feedback was considered in preliminary studies related to the control system for the NASA Shuttle Remote Manipulator System (RMS) by Golla, Garg and Hughes.[25] A feature of our work is that for the fast subsystem, deriving signals from the strain gauges has been avoided. The nonlinear equations of the fast subsystem for a flexible manipulator have been treated as linear equations with time-varying parameters under the assumption that the flexibility variables vary at a faster rate than the joint variables. After these equations have been put into state variable form and discretized, the fast subsystem and input matrix have a structure that permits simplification of the procedure for finding the block companion form for the flexible subsystem. Finally, we have reduced the determination of the state feedback gains to the evaluation of explicit expressions requiring only two matrix multiplications. The theoretical and experimental results obtained in this paper will show that if control motors with motor drivers of speed reference type are used and the strain signals at the root ends of the flexible links are measured and directly fed back, then the vibrations can be controlled. The remains of this paper is organized as follows:

In Section 2 the experimental setup is briefly described. The dynamic and kinematic models are introduced in Section 3. In Section 4, a brief description of a velocity servo loop is given, and a gross motion control law based upon Cartesian-based errors is proposed. In Section 5, we propose a pole assignment method for damping out vibrations in which only the strain signals need to be measured. Laboratory experiments are shown to demonstrate control performances of the presented method in Section 6. Finally, some discussions and conclusions are drawn in Section 7 and 8.

2. A SPATIAL FLEXIBLE MANIPULATOR

A three-link, spatial flexible manipulator has been designed and experimented in the Spacecraft Systems Laboratory, as shown in Figure 1. The first link is mounted vertically and rotates about its base. This link is short and fat and is considered to be rigid. The other two links are slender and are fairly flexible. They undergo transverse and torsional vibrations as they move. Coordinate systems are defined according to Paul's convention. A payload is represented by a point-mass of 0.3 [kg] located at the tip of the third link. This robot is a real apparatus named FLEBOT II (FLExible roBOT II) in the Spacecraft Systems Laboratory of the Department of Aeronautics and Space Engineering at Tohoku University.[19–26] Each motor is connected to a harmonic drive reduction gear and is controlled by a hardware velocity servo card using tachometer feedback. Encoders are built in to measure joint angles, and strain gauges located at the root ends of the flexible rods measure the elastic deflections. The three links are driven by three DC servo motors with gear down ratios 100 : 1, 100 : 1, and 80 : 1, respectively. The second and third links are made of elastic steel materials (SWP-A) with weights 166 g and 81 g, respectively. The shapes of the last two links are solid rods with radii 4 mm and 3 mm, respectively.

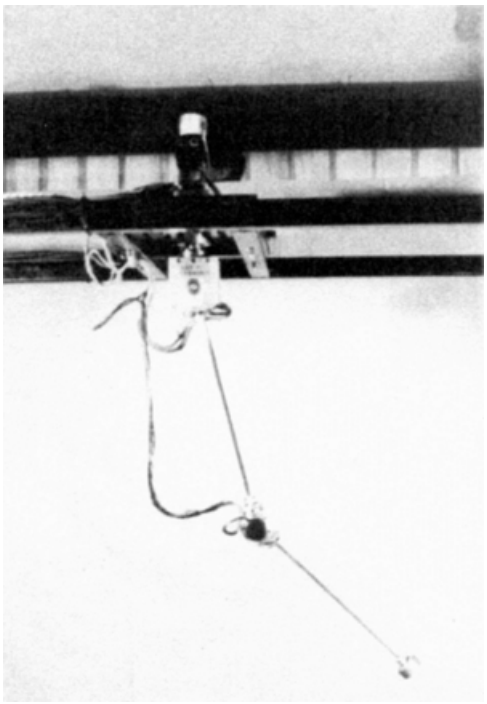

Fig. 1. A three-link, spatial manipulator.

For sensing the bending deflections of each link, a two-strain gauge method is used to gain high sensitivity and eliminate the torsional influences. For measuring the link torsional deflections, a four-strain gauge method is employed to acquire high sensitivity and eliminate the bending effects. Signals from the strain gauges will first be regulated by bridge circuits to compensate for drifts, and then be amplified as the input to an A/D converter. Also, the high frequency modes are filtered by an appropriately designed low-pass filter. After that, they are read by a computer for control purposes. Table I lists the values of the properties, and Table II shows the properties of the actuators.

Table I. Properties of links.

Parameter	Notation	Value
Length of links	L_2 [m]	0.50
	L_3 [m]	0.14
Bending stiffness	E_2I_2 [Nm^2]	41.82
	E_3I_3 [Nm^2]	13.23
Torsional stiffness	G_2J_2 [Nm^2]	32.17
	G_3J_3 [Nm^2]	10.18
Mass of joints	m_2 [kg]	4.0
	m_3 [kg]	1.5
Payload	m_p [kg]	0.3

https://doi.org/10.1017/S0263574702004435 Published online by Cambridge University Press

Table II. Properties of actuators.

Parameter	Notation	Value
Velocity feedback gains	Ψ_1 [Nm/V]	150.7
	Ψ_2 [Nm/V]	150.7
	Ψ_3 [Nm/V]	38.9
Back e.m.f. coefficients	Ω_1 [Vs/rad]	2.86
	Ω_2 [Vs/rad]	2.86
	Ω_3 [Vs/rad]	2.52
Inertia of motors	I_{m1} [kgm^2]	0.326
	I_{m2} [kgm^2]	0.326
	I_{m3} [kgm^2]	0.041

The programming enviroment for control software development consists of a UNIX host machine and a target computer which deals with the signals from sensors and calculates the command to control the movement of the joints. Our particular host is a Sun Enterprise Ultra 10S Server with Solaris 2.6 as its operating system, and our target computer is a Pentium running a VxWorks 5.3.1 shell. The control program was written in the *C* computer language. The two computers are able to communicate with each other over the Ethernet. Once the source code has been compiled to object code on the host machine, it can be downloaded to the target computer where it is linked with any other relevant object code, and transformed into an executable code. At this point, programs can be executed by giving a corresponding function name.

3. KINEMATICS AND DYNAMICS

Now let us consider a manipulator having flexible links connected by rigid joints. The location of the end-effector of a flexible manipulator can be obtained by combining the link deflections with the location of the rigid-link counterpart of the flexible-link manipulator. That is to say, the position of the end-effector with respect to the base frame is a function of both rigid and flexible degrees of freedom, as seen in Figure 2.

The position of the end-effector with a response to the base frame is a function of both rigid and flexible degrees of freedom

$$\boldsymbol{p}=\boldsymbol{f}(\boldsymbol{\theta}, \boldsymbol{e}) \tag{1}$$

where, vectors $\boldsymbol{p}\in\mathrm{R}^m$, $\boldsymbol{\theta}\in\mathrm{R}^{n_r}$ and $\boldsymbol{e}\in\mathrm{R}^{n_f}$ represent the generalized position of the end-effector, the joint variables and the link elastic deflection, respectively. With the definitions given in Figure 2, $\boldsymbol{p}$, $\boldsymbol{\theta}$, and $\boldsymbol{e}$ attached to FLEBOT II can be expressed as $\boldsymbol{p}=[p_x\ p_y\ p_z]^T$, $\boldsymbol{\theta}=[\theta_1\ \theta_2\ \theta_3]^T$, and $\boldsymbol{e}=[e_{y2}\ e_{y3}\ e_{z2}\ e_{z3}]^T$, respectively. Deflectional angles are, in fact, dependent variables with $\boldsymbol{e}$, as seen in the Appendix, e_{y2} and e_{y3} are thought to be vertical deflections, e_{z2} and e_{z3} are horizontal deflections.[4, 26]

The end-effector velocity is obtained by differentiating (1) with respect to time

$$\dot{\boldsymbol{p}}=\frac{\partial \boldsymbol{f}}{\partial \boldsymbol{\theta}}\dot{\boldsymbol{\theta}}+\frac{\partial \boldsymbol{f}}{\partial \boldsymbol{e}}\dot{\boldsymbol{e}}. \tag{2}$$

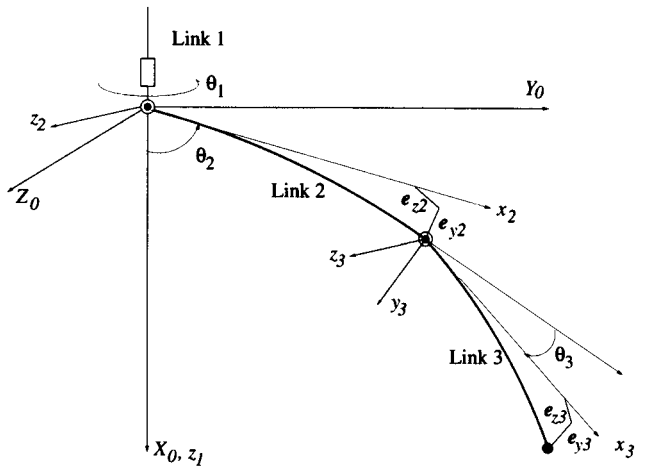

Fig. 2. Definition of deflections.

Let

$$\boldsymbol{J}_\theta=\frac{\partial \boldsymbol{f}}{\partial \boldsymbol{\theta}} \tag{3}$$

the rigid Jacobian matrix, and

$$\boldsymbol{J}_e=\frac{\partial \boldsymbol{f}}{\partial \boldsymbol{e}} \tag{4}$$

the flexible Jacobian matrix. Equation (2) then becomes

$$\dot{\boldsymbol{p}}=\boldsymbol{J}_\theta\dot{\boldsymbol{\theta}}+\boldsymbol{J}_e\dot{\boldsymbol{e}}. \tag{5}$$

Differentiating (5), we obtain the differential relation for accelerations

$$\ddot{\boldsymbol{p}}=\boldsymbol{J}_\theta\ddot{\boldsymbol{\theta}}+\boldsymbol{J}_e\ddot{\boldsymbol{e}}+\dot{\boldsymbol{J}}_\theta\dot{\boldsymbol{\theta}}+\dot{\boldsymbol{J}}_e\dot{\boldsymbol{e}}. \tag{6}$$

In the case of FLEBOT II, $m=n_r=3$, $n_f=4$, and $\boldsymbol{J}_\theta$ is guaranteed to be a square matrix.

The dynamics of a system of multiple flexible link manipulators can be described by the set of equations:

$$\begin{aligned}&\boldsymbol{M}_{11}(\boldsymbol{\theta}, \boldsymbol{e})\ddot{\boldsymbol{\theta}}+\boldsymbol{M}_{12}(\boldsymbol{\theta}, \boldsymbol{e})\ddot{\boldsymbol{e}}\\&\quad+\boldsymbol{h}_1(\boldsymbol{\theta}, \dot{\boldsymbol{\theta}}, \boldsymbol{e}, \dot{\boldsymbol{e}})+\boldsymbol{g}_1(\boldsymbol{\theta}, \boldsymbol{e})=\tau,\end{aligned} \tag{7}$$

$$\begin{aligned}&\boldsymbol{M}_{21}(\boldsymbol{\theta}, \boldsymbol{e})\ddot{\boldsymbol{\theta}}+\boldsymbol{M}_{22}(\boldsymbol{\theta}, \boldsymbol{e})\ddot{\boldsymbol{e}}\\&\quad+\boldsymbol{h}_2(\boldsymbol{\theta}, \dot{\boldsymbol{\theta}}, \boldsymbol{e}, \dot{\boldsymbol{e}})+\boldsymbol{g}_2(\boldsymbol{\theta}, \boldsymbol{e})+\boldsymbol{K}_{22}(\boldsymbol{\theta})\boldsymbol{e}=\boldsymbol{0}.\end{aligned} \tag{8}$$

τ denotes the $n_r\times 1$ vector of applied torques, where $\boldsymbol{M}_{11}\in\mathrm{R}^{n_r\times n_r}$, $\boldsymbol{M}_{12}\in\mathrm{R}^{n_r\times n_f}$, $\boldsymbol{M}_{21}\in\mathrm{R}^{n_f\times n_r}$, and $\boldsymbol{M}_{22}\in\mathrm{R}^{n_f\times n_f}$ are block matrices that form the $(n_r+n_f)\times(n_r+n_f)$ configuration-dependent generalized mass matrix, $\boldsymbol{h}_1$ and $\boldsymbol{h}_2$ are the $n_r\times 1$ and $n_f\times 1$ vectors of Coriolis and centrifugal terms and the terms accounting for the interaction of joint variables and their rates with flexible variables and their rates, respectively. $\boldsymbol{g}_1$ and $\boldsymbol{g}_2$ are the $n_r\times 1$ and $n_f\times 1$ vectors of gravitational terms, $\boldsymbol{K}_{22}$ is the $n_f\times n_f$ flexible structure stiffness matrix of the system. Part of the kinematic and dynamic model of spatial flexible manipulator, FLEBOT II, is presented in the Appendix, the interested reader is referred to reference 26 for full details.

4. SINGULARLY PERTURBED EQUATIONS

Figure 3 shows the feedback diagram of the hardware velocity servo loop for joint *i*. The servo system of the

https://doi.org/10.1017/S0263574702004435 Published online by Cambridge University Press

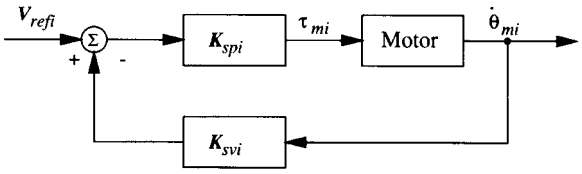

Fig. 3. Hardware velocity servo loop.

motor driver is of a high internal gain speed reference type. From this figure, we obtain the following equation

$$\tau_{mi}=K_{spi}(V_{refi}-K_{svi}\dot{\theta}_{mi}), \quad i=1, \ldots, n_r \tag{9}$$

where τ_{mi} is the torque applied by the ith motor, $\dot{\theta}_{mi}$ is the motor velocity, V_{refi} is the voltage corresponding to the commanded velocity, K_{svi} is the voltage/velocity coefficient, and K_{spi} is the voltage feedback gain.

If the gear reduction ratio is N_i, and using the relations $\tau_i=N_i\tau_{mi}$ and $\dot{\theta}_i=\dot{\theta}_{mi}/N_i$, then the torque applied at joint i is:

$$\tau_i=\Psi_i(V_{refi}-\Omega_i\dot{\theta}_i), \quad i=1, \ldots, n_r \tag{10}$$

where $\dot{\theta}_i$ is the joint velocity, $\Psi_i=N_iK_{spi}$ is the velocity feedback gain, $\Omega_i=N_iK_{svi}$ is the back electromotive force (e.m.f.) coefficient. Equation (10) can be rewritten as

$$\boldsymbol{\tau}=\boldsymbol{\Psi}(\boldsymbol{V}_{ref}-\boldsymbol{\Omega}\dot{\boldsymbol{\theta}}) \tag{11}$$

where $\boldsymbol{\Psi}=\mathrm{diag}(\Psi_i)$, $\boldsymbol{\Omega}=\mathrm{diag}(\Omega_i)$, and $\boldsymbol{N}=\mathrm{diag}(N_i)$, for $i=1, \ldots, n_r$.

Most of the reported experimental flexible manipulators use torque motors to provide a fast control response and linearity;[28, 29] very few velocity input control schemes have been published in the literature.[26, 30] If we choose servo motors with motor drives of a high gain speed reference type, the input voltages $\boldsymbol{V}_{ref}(t)$ to the motor drives are approximately proportional to angular velocities $\dot{\boldsymbol{\theta}}(t)$ of the motors, i.e.,

$$\boldsymbol{V}_{ref}\doteq\boldsymbol{\Omega}\dot{\boldsymbol{\theta}} \tag{12}$$

where $\boldsymbol{\Omega}$ is the back e.m.f. constant matrix of the motors.

Since the voltage input $\boldsymbol{V}_{ref}$ consists of two terms, one ($\boldsymbol{V}_{refg}$) is computed to drive the end-effector to follow the planned trajectory, the other ($\boldsymbol{V}_{reff}$) is calculated to cancel vibrations caused by the structural flexibility of flexible link manipulators; $\boldsymbol{V}_{ref}$ can be expressed as $\boldsymbol{V}_{ref}=\boldsymbol{V}_{refg}+\boldsymbol{V}_{reff}$.

Provided that kinematic singularities are avoided and the flexible manipulator is required to work within its legitimate envelope, then, we consider a gross motion control law in a Cartesian space which drives the end-effector of the flexible manipulator to follow the planned trajectory as closely as possible:

$$\boldsymbol{V}_{refg}=\boldsymbol{\Omega}\boldsymbol{J}_{\theta}^{-1}(\boldsymbol{\theta}, \boldsymbol{e})\{\dot{\boldsymbol{p}}_d+\boldsymbol{K}_P(\boldsymbol{p}_d-\boldsymbol{p}) +\boldsymbol{K}_I\int_0^t(\boldsymbol{p}_d-\boldsymbol{p})dt\} \tag{13}$$

where $\boldsymbol{p}_d(t)$ denotes a given desired path, and feedback gains $\boldsymbol{K}_P$, $\boldsymbol{K}_I$ are positive definite constant matrices. With appropriate gain matrices $\boldsymbol{K}_P$, $\boldsymbol{K}_I$ the motion of the flexible manipulator follows in a neighborhood of the given desired output. From (13), it can be seen that the gross control method proposed does not require a derivative of the end-effector's position, i.e. the velocity of end-effector is not needed. As to the measurement of the end-effector's position (i.e, $\boldsymbol{p}$), a camera or a set of laser PSDs can be used to sense the position directly. In the reference 31, a Landmark Tracking System and lateral-effect photodiodes are used to measure the end-point position of the flexible manipulator. For simplicity, in this paper the end-effector's position is calculated according to Equation (1), using the joint angles measured by encoders and the link deflections measured by strain gauges.

In order to make control design simpler, we separate the rigid subsystem and the flexible subsystem of flexible manipulator by using a singular perturbation method to derive controllers for the rigid subsystem and the flexible subsystem separately. Since we have already given a PI control law Equation (13) for trajectory tracking of an end-effector based on Cartesian space errors, the following focus is only on deriving controller for the flexible subsystem (i.e. fast subsystem).

Following Marino and Nicosia,[32] singularly perturbed equations can be obtained as follows: Assume that the orders of magnitude of the k_{ij} are comparable. It is then appropriate to extract a common scale factor k (the smallest spring constant of stiff matrix $\boldsymbol{K}_{22}(\boldsymbol{\theta})$, for example) such that

$$k_{ij}=k\tilde{k}_{ij}, \quad i, j=1, \ldots, n_f. \tag{14}$$

The following new variables (elastic forces) can be defined

$$\boldsymbol{\zeta}=k\boldsymbol{e}, \quad \boldsymbol{K}_{22}(\boldsymbol{\theta})=k\widetilde{\boldsymbol{K}}_{22}(\boldsymbol{\theta}), \tag{15}$$

$$\widetilde{\boldsymbol{K}}_{22}(\boldsymbol{\theta})=\begin{bmatrix}\tilde{k}_{11} & \ldots & \tilde{k}_{1n_f}\\ \vdots & \ddots & \vdots\\ \tilde{k}_{n_f1} & \ldots & \tilde{k}_{n_fn_f}\end{bmatrix} \tag{16}$$

The next step is to define $\mu=1/k$, from Equation (8), we obtain

$$\boldsymbol{M}_{21}(\boldsymbol{\theta}, \mu\boldsymbol{\zeta})\ddot{\boldsymbol{\theta}}+\boldsymbol{M}_{22}(\boldsymbol{\theta}, \mu\boldsymbol{\zeta})\mu\ddot{\boldsymbol{\zeta}} +\boldsymbol{h}_2(\boldsymbol{\theta}, \dot{\boldsymbol{\theta}}, \mu\boldsymbol{\zeta}, \mu\dot{\boldsymbol{\zeta}})+\boldsymbol{g}_2(\boldsymbol{\theta}, \mu\boldsymbol{\zeta})+\widetilde{\boldsymbol{K}}_{22}(\boldsymbol{\theta})\boldsymbol{\zeta}=0 \tag{17}$$

which are singularly perturbed equations of the flexible manipulator. μ is obtained as the inverse of the smallest flexural spring constant.

The joint accelerations $\ddot{\boldsymbol{\theta}}$ are composed of two parts, one (expressed by $\ddot{\bar{\boldsymbol{\theta}}}$) is contributed to producing joint angle $\bar{\boldsymbol{\theta}}$, and velocity $\dot{\bar{\boldsymbol{\theta}}}$, the other (expressed by $\ddot{\boldsymbol{\vartheta}}$) is responsible for damping out vibrations excited due to link flexibility during and at the end of motion.[4, 26, 27]

Setting $\mu=0$ and solving for ζ in Eqaution (17), we have

$$\boldsymbol{M}_{21}(\bar{\boldsymbol{\theta}}, \boldsymbol{0})\ddot{\bar{\boldsymbol{\theta}}}+\boldsymbol{h}_2(\bar{\boldsymbol{\theta}}, \dot{\bar{\boldsymbol{\theta}}}, \boldsymbol{0}, \boldsymbol{0})+\boldsymbol{g}_2(\bar{\boldsymbol{\theta}}, \boldsymbol{0})+\widetilde{\boldsymbol{K}}_{22}(\bar{\boldsymbol{\theta}})\bar{\boldsymbol{\zeta}}=\boldsymbol{0}. \tag{18}$$

where the overlines are utilized to denote that the system with $\mu=0$ is considered.

Now,[33, 34] choosing $z_1=\boldsymbol{\zeta}$, $z_2=\epsilon\dot{\boldsymbol{\zeta}}$ with $\epsilon=\sqrt{\mu}$ gives the state-space form of the equation (17), i.e.

$$\begin{aligned}\epsilon\dot{z}_1&=z_2,\\ \epsilon\dot{z}_2&=-\boldsymbol{M}_{22}^{-1}(\boldsymbol{\theta}, \epsilon^2 z_1)\{\boldsymbol{h}_2(\boldsymbol{\theta}, \dot{\boldsymbol{\theta}}, \epsilon^2 z_1, \epsilon z_2)\\ &\quad+\boldsymbol{g}_2(\boldsymbol{\theta}, \epsilon^2 z_1)+\widetilde{\boldsymbol{K}}_{22}(\boldsymbol{\theta})z_1+\boldsymbol{M}_{21}(\boldsymbol{\theta}, \epsilon^2 z_1)\ddot{\boldsymbol{\theta}}\}.\end{aligned} \tag{19}$$

To derive the fast subsystem, we introduced the fast time scale $\tau=t/\epsilon$. Then it can be seen that the Equation (19) in the fast time scale becomes

https://doi.org/10.1017/S0263574702004435 Published online by Cambridge University Press

$$\frac{d\boldsymbol{\eta}_1}{d\tau}=\boldsymbol{\eta}_2,$$

$$\frac{d\boldsymbol{\eta}_2}{d\tau}=-\boldsymbol{M}_{22}^{-1}(\boldsymbol{\theta},\epsilon^2(\boldsymbol{\eta}_1+\bar{\boldsymbol{\zeta}}))\{$$
$$\boldsymbol{h}_2(\boldsymbol{\theta},\dot{\boldsymbol{\theta}},\epsilon^2(\boldsymbol{\eta}_1+\bar{\boldsymbol{\zeta}}),\epsilon\boldsymbol{\eta}_2)$$
$$+\boldsymbol{g}_2(\boldsymbol{\theta},\epsilon^2(\boldsymbol{\eta}_1+\bar{\boldsymbol{\zeta}}))+\widetilde{\boldsymbol{K}}_{22}(\boldsymbol{\theta})(\boldsymbol{\eta}_1+\bar{\boldsymbol{\zeta}})$$
$$+\boldsymbol{M}_{21}(\boldsymbol{\theta},\epsilon^2(\boldsymbol{\eta}_1+\bar{\boldsymbol{\zeta}}))\ddot{\boldsymbol{\theta}}\}. \tag{20}$$

where the new fast variables $\boldsymbol{\eta}_1$ and $\boldsymbol{\eta}_2$ are defined as

$$\boldsymbol{\eta}_1=z_1-\bar{\boldsymbol{\zeta}},$$
$$\boldsymbol{\eta}_2=z_2. \tag{21}$$

From Equation (12), we have

$$\frac{d\boldsymbol{\theta}}{d\tau}=\epsilon\boldsymbol{\Omega}^{-1}\boldsymbol{V}_{ref} \tag{22}$$

Now setting $\epsilon=0$ in Equation (22) yields $d\boldsymbol{\theta}/d\tau=\boldsymbol{0}$; i.e. $\boldsymbol{\theta}$ is constant in the boundary layer. Therefore, letting $\epsilon=0$ in Equation (20) and by using Equation (18) the fast subsystem can be found to be

$$\frac{d\boldsymbol{\eta}_1}{d\tau}=\boldsymbol{\eta}_2,$$

$$\frac{d\boldsymbol{\eta}_2}{d\tau}=-\boldsymbol{M}_{22}^{-1}(\bar{\boldsymbol{\theta}},\boldsymbol{0})\widetilde{\boldsymbol{K}}_{22}(\bar{\boldsymbol{\theta}})\boldsymbol{\eta}_1 \tag{23}$$
$$-\boldsymbol{M}_{22}^{-1}(\bar{\boldsymbol{\theta}},\boldsymbol{0})\boldsymbol{M}_{21}(\bar{\boldsymbol{\theta}},\boldsymbol{0})\ddot{\boldsymbol{\vartheta}}$$

which is a linear system parametrized in the slow variables $\bar{\boldsymbol{\theta}}$. In (23) $\ddot{\boldsymbol{\vartheta}}$ will be used to design a vibrations controller.

Let $\boldsymbol{\chi}_1$ and $\boldsymbol{\chi}_2$ be integrals of $\boldsymbol{\eta}_1$ and $\boldsymbol{\eta}_2$ within the boundary layer, respectively. Integrating Equation (22) by using Equation (12) and assumed that all initial values are zero, we obtain

$$\frac{d\boldsymbol{\chi}_1}{d\tau}=\boldsymbol{\chi}_2,$$

$$\frac{d\boldsymbol{\chi}_2}{d\tau}=-\boldsymbol{M}_{22}^{-1}(\bar{\boldsymbol{\theta}},\boldsymbol{0})\widetilde{\boldsymbol{K}}_{22}(\bar{\boldsymbol{\theta}})\boldsymbol{\chi}_1 \tag{24}$$
$$-\boldsymbol{M}_{22}^{-1}(\bar{\boldsymbol{\theta}},\boldsymbol{0})\boldsymbol{M}_{21}(\bar{\boldsymbol{\theta}},\boldsymbol{0})\boldsymbol{\Omega}^{-1}\boldsymbol{V}_{reff}(\bar{\boldsymbol{\theta}},\boldsymbol{\chi}_1,\boldsymbol{\chi}_2)$$

where $\boldsymbol{V}_{reff}(\bar{\boldsymbol{\theta}},\boldsymbol{\chi}_1,\boldsymbol{\chi}_2)$ with the constraint that $\boldsymbol{V}_{reff}(\bar{\boldsymbol{\theta}},\boldsymbol{0},\boldsymbol{0})=\boldsymbol{0}$ such that $\boldsymbol{V}_{reff}$ is inactive along the motion (18), which is then an equilibrium trajectory of Equation (17). A composite input is formed with $\boldsymbol{V}_{ref}=\boldsymbol{V}_{refg}+\boldsymbol{V}_{reff}$, in which $\boldsymbol{V}_{refg}$ is designed to drive the end-effector of a flexible manipulator to track the preplanned trajectory; $\boldsymbol{V}_{reff}$ is responsible for damping out unwanted vibrations during and at the end of trajectory tracking.

In the strict sense of the word, there are some similarities and differences between our method and the singular perturbation method:[11–14]

- In our method, the whole dynamic system of flexible manipulator has not been separated into two subsystems, i.e. the rigid subsystem (or slow subsystem) and the flexible subsystem (or fast subsystem). Instead, only the flexible subsystem has been derived. A gross motion control law is proposed in advance of obtaining the flexible subsystem from the whole dynamic system.
- In our method, the gross motion control law designed for trajectory tracking control is involved in the value ($\boldsymbol{e}$) which belongs to the flexible subsystem.
- In our method, the slow variables, for example joint angles $\boldsymbol{\theta}$, are not controlled directly. Although the end-effector's position is controlled directly, joint angles $\boldsymbol{\theta}$ are related to the controlled end-effector's position through Equation (1).

5. POLE ASSIGNMENT CONTROL OF VIBRATIONS

Some researchers used a singular perturbation approach to control the rigid subsystem and the flexible subsystem separately in which a two-time scale assumption is employed.[11, 12] In the above section, we have already obtained a state-space form flexible subsystem. In this section, we use the pole assignment method to control vibrations. The corresponding more compact representation of Equation (24) is written as

$$\dot{\boldsymbol{\chi}}=\boldsymbol{A}\boldsymbol{\chi}+\boldsymbol{B}\boldsymbol{V}'_{reff} \tag{25}$$

where $\boldsymbol{\chi}=[\boldsymbol{\chi}_1\ \boldsymbol{\chi}_2]^T$, and $\boldsymbol{V}'_{reff}$ is a new $n_f\times 1$ input vector which is introduced to simplify the following derivation, where

$$\boldsymbol{V}'_{reff}=-\boldsymbol{M}_{21}(\bar{\boldsymbol{\theta}},\boldsymbol{0})\boldsymbol{\Omega}^{-1}\boldsymbol{V}_{reff} \tag{26}$$

and

$$\boldsymbol{A}=\begin{bmatrix}\boldsymbol{0} & \boldsymbol{I}\\ -\boldsymbol{M}_{22}^{-1}(\bar{\boldsymbol{\theta}},\boldsymbol{0})\widetilde{\boldsymbol{K}}_{22}(\bar{\boldsymbol{\theta}}) & \boldsymbol{0}\end{bmatrix},\quad \boldsymbol{B}=\begin{bmatrix}\boldsymbol{0}\\ \boldsymbol{M}_{22}^{-1}(\bar{\boldsymbol{\theta}},\boldsymbol{0})\end{bmatrix}. \tag{27}$$

For digital control, we must discretize the equations of motion. The system is discretized by using an Euler approximation with a sampling interval of time T_s to obtain

$$\boldsymbol{\chi}(k+1)=\boldsymbol{G}\boldsymbol{\chi}(k)+\boldsymbol{H}\boldsymbol{V}'_{reff}(k) \tag{28}$$

where $\boldsymbol{G}=\boldsymbol{I}+\boldsymbol{A}T_s$, and $\boldsymbol{H}=\boldsymbol{B}T_s$. Here, k represents kT_s instant.

The control law is given as follows:

$$\boldsymbol{V}'_{reff}(k)=-\boldsymbol{K}\boldsymbol{\chi}(k) \tag{29}$$

and $\boldsymbol{K}=[\boldsymbol{K}_1\ \boldsymbol{K}_2]$ is an $n_f\times 2n_f$ gain matrix. In a block companion form the state equations are

$$\boldsymbol{\chi}_c(k+1)=\boldsymbol{G}_c\boldsymbol{\chi}_c(k)+\boldsymbol{H}_c\boldsymbol{V}'_{reff}(k) \tag{30}$$

where $\boldsymbol{\chi}_c(k)$ is the state vector expressed in the transformed coordinates, and T_c is the transformation matrix defined by

$$\boldsymbol{\chi}_c(k)=\boldsymbol{T}_c\boldsymbol{\chi}(k) \tag{31}$$

where

$$\boldsymbol{T}_c=\begin{bmatrix}\boldsymbol{T}_{c1}\\ \boldsymbol{T}_{c2}\end{bmatrix}=\begin{bmatrix}\boldsymbol{T}_{c1}\\ \boldsymbol{T}_{c1}\boldsymbol{G}\end{bmatrix} \tag{32}$$

https://doi.org/10.1017/S0263574702004435 Published online by Cambridge University Press

and

$$\boldsymbol{T}_{c1}=[\boldsymbol{0}\ \boldsymbol{I}][\boldsymbol{H}\ \boldsymbol{GH}]^{-1}. \tag{33}$$

For a flexible manipulator the flexible subsystem and input matrices are

$$\boldsymbol{G}=\begin{bmatrix} \boldsymbol{I} & T_s\boldsymbol{I} \\ -\boldsymbol{M}_{22}^{-1}(\bar{\boldsymbol{\theta}},\boldsymbol{0})\widetilde{\boldsymbol{K}}_{22}(\bar{\boldsymbol{\theta}})T_s & \boldsymbol{I} \end{bmatrix}, \tag{34}$$

$$\boldsymbol{H}=\begin{bmatrix} \boldsymbol{0} \\ \boldsymbol{M}_{22}^{-1}(\bar{\boldsymbol{\theta}},\boldsymbol{0})T_s \end{bmatrix} \tag{35}$$

where $\boldsymbol{M}_{22}^{-1}(\bar{\boldsymbol{\theta}},\boldsymbol{0})$ is an $n_f\times n_f$ nonsingular matrix.[35] Thus we obtain

$$\boldsymbol{T}_c=\begin{bmatrix} \boldsymbol{M}_{22}(\bar{\boldsymbol{\theta}},\boldsymbol{0})T_s^{-2} & \boldsymbol{0} \\ \boldsymbol{M}_{22}(\bar{\boldsymbol{\theta}},\boldsymbol{0})T_s^{-2} & \boldsymbol{M}_{22}(\bar{\boldsymbol{\theta}},\boldsymbol{0})T_s^{-1} \end{bmatrix}. \tag{36}$$

It can be easily verified that

$$\boldsymbol{T}_c^{-1}=\begin{bmatrix} \boldsymbol{M}_{22}^{-1}(\bar{\boldsymbol{\theta}},\boldsymbol{0})T_s^2 & \boldsymbol{0} \\ -\boldsymbol{M}_{22}^{-1}(\bar{\boldsymbol{\theta}},\boldsymbol{0})T_s & \boldsymbol{M}_{22}^{-1}(\bar{\boldsymbol{\theta}},\boldsymbol{0})T_s \end{bmatrix}. \tag{37}$$

From Equations (30) and (31), we have

$$\boldsymbol{G}_c=\boldsymbol{T}_c\boldsymbol{G}\boldsymbol{T}_c^{-1}=\begin{bmatrix} \boldsymbol{0} & \boldsymbol{I} \\ \boldsymbol{G}_{c1} & \boldsymbol{G}_{c2} \end{bmatrix}. \tag{38}$$

$$\boldsymbol{H}_c=\boldsymbol{T}_c\boldsymbol{H}=[\boldsymbol{0}\quad \boldsymbol{I}]^T \tag{39}$$

where

$$\begin{cases} \boldsymbol{G}_{c1}=-\boldsymbol{I}-\widetilde{\boldsymbol{K}}_{22}(\bar{\boldsymbol{\theta}})\boldsymbol{M}_{22}^{-1}(\bar{\boldsymbol{\theta}},\boldsymbol{0})T_s^2 \\ \boldsymbol{G}_{c2}=2\boldsymbol{I}. \end{cases} \tag{40}$$

The block companion form simplifies the determination of gains corresponding to the pole placement. In this case the gain matrix $\boldsymbol{K}_c=[\boldsymbol{K}_{c1}\ \boldsymbol{K}_{c2}]$ is found such that

$$\det(z\boldsymbol{I}-(\boldsymbol{G}_c-\boldsymbol{H}_c\boldsymbol{K}_c))=\det(z\boldsymbol{I}-\boldsymbol{\Lambda}) \tag{41}$$

where z is the z-transform operator, and $\boldsymbol{\Lambda}$ is a $2n_f\times 2n_f$ diagonal matrix with the desired poles as entries on the main diagonal. The above equation can be written in the form

$$\det\left(z\boldsymbol{I}-\begin{bmatrix} \boldsymbol{0} & \boldsymbol{I} \\ \boldsymbol{G}_{c1}-\boldsymbol{K}_{c1} & \boldsymbol{G}_{c2}-\boldsymbol{K}_{c2} \end{bmatrix}\right)$$

$$=\det\left(z\boldsymbol{I}-\begin{bmatrix} \boldsymbol{\Lambda}_1 & \boldsymbol{0} \\ \boldsymbol{0} & \boldsymbol{\Lambda}_2 \end{bmatrix}\right). \tag{42}$$

Therefore

$$\begin{cases} \boldsymbol{G}_{c1}-\boldsymbol{K}_{c1}=-\boldsymbol{\Lambda}_1\boldsymbol{\Lambda}_2 \\ \boldsymbol{G}_{c2}-\boldsymbol{G}_{c2}=\boldsymbol{\Lambda}_1+\boldsymbol{\Lambda}_2 \end{cases} \tag{43}$$

and

$$\begin{cases} \boldsymbol{K}_{c1}=\boldsymbol{G}_{c1}+\boldsymbol{\Lambda}_1\boldsymbol{\Lambda}_2 \\ \boldsymbol{K}_{c2}=\boldsymbol{G}_{c2}-(\boldsymbol{\Lambda}_1+\boldsymbol{\Lambda}_2). \end{cases} \tag{44}$$

The gain is then transformed back into the original coordinates by post-multiplying $\boldsymbol{K}_c$ by $\boldsymbol{T}_c$, i.e.

$$\boldsymbol{K}=\boldsymbol{K}_c\boldsymbol{T}_c. \tag{45}$$

By combining Equations (40), (44) and (45), we obtain

$$\begin{cases} \boldsymbol{K}_1=[\boldsymbol{I}-(\boldsymbol{\Lambda}_1+\boldsymbol{\Lambda}_2)+\boldsymbol{\Lambda}_1\boldsymbol{\Lambda}_2]\boldsymbol{M}_{22}(\bar{\boldsymbol{\theta}},\boldsymbol{0})T_s^{-2}-\widetilde{\boldsymbol{K}}_{22}(\bar{\boldsymbol{\theta}}) \\ \boldsymbol{K}_2=[2\boldsymbol{I}-(\boldsymbol{\Lambda}_1+\boldsymbol{\Lambda}_2)]\boldsymbol{M}_{22}(\bar{\boldsymbol{\theta}},\boldsymbol{0})T_s^{-1}. \end{cases} \tag{46}$$

Given the matrix $\boldsymbol{M}_{22}(\bar{\boldsymbol{\theta}},\boldsymbol{0})$ of flexible subsystem parameters and the matrix of desired poles, the computation of the controller gains only requires two matrix multiplications and one matrix subtraction.

From equation (26), we have

$$\boldsymbol{V}_{reff}=\boldsymbol{\Omega}\boldsymbol{M}_{21}^{+}(\bar{\boldsymbol{\theta}},\boldsymbol{0})[\boldsymbol{K}_1\boldsymbol{\chi}_1+\boldsymbol{K}_2\boldsymbol{\chi}_2] \tag{47}$$

where $\boldsymbol{M}_{21}^{+}(\bar{\boldsymbol{\theta}},\boldsymbol{0})$ denotes the pseudo-inverse of $\boldsymbol{M}_{21}(\bar{\boldsymbol{\theta}},\boldsymbol{0})$ which is represented as follows:

$$\boldsymbol{M}_{21}^{+}=\begin{cases} (\boldsymbol{M}_{21}^T\boldsymbol{M}_{21})^{-1}\boldsymbol{M}_{21}^T & n_f>n_r \\ \boldsymbol{M}_{21}^T(\boldsymbol{M}_{21}\boldsymbol{M}_{21}^T)^{-1} & n_f<n_r \\ \boldsymbol{M}_{21}^{-1} & n_f=n_r \end{cases} \tag{48}$$

Usually, we select closed-loop poles as $\boldsymbol{\Lambda}_{1,2}=\mathrm{diag}(a_i\pm b_ij)$, $i=1,\ldots,n_f$, which are satisfied on condition under which all poles are located inside unit cycle.

Figure 4 shows the overall block diagram of control system.

6. EXPERIMENTAL RESULTS

The proposed control strategy will be now studied by a series of experiments. The desired trajectory is directly described in the Cartesian coordinates as

$$\boldsymbol{p}_d=[p_{xd}\ p_{yd}\ p_{zd}]^T \tag{49}$$

where

$$\begin{cases} p_{xd}(t)=59+9\sin(2\pi s(t))\ [\mathrm{cm}] \\ p_{yd}(t)=59-9\cos(2\pi s(t))\ [\mathrm{cm}] \\ p_{zd}(t)=9\sin(2\pi s(t))\ [\mathrm{cm}] \end{cases} \tag{50}$$

and $s(t)$ is a fifth order polynomial

$$s(t)=10\left(\frac{t}{T}\right)^3-15\left(\frac{t}{T}\right)^4+6\left(\frac{t}{T}\right)^5,\quad 0\le t\le \mathrm{T} \tag{51}$$

where $T=4$ [s] is the expected duration of motion; the gain matrices used in this experiment are

$$\boldsymbol{K}_P=\begin{bmatrix} 8 & \boldsymbol{0} \\ & 8 \\ \boldsymbol{0} & 4 \end{bmatrix},\quad \boldsymbol{K}_1=\begin{bmatrix} 16 & \boldsymbol{0} \\ & 16 \\ \boldsymbol{0} & 8 \end{bmatrix}. \tag{52}$$

https://doi.org/10.1017/S0263574702004435 Published online by Cambridge University Press

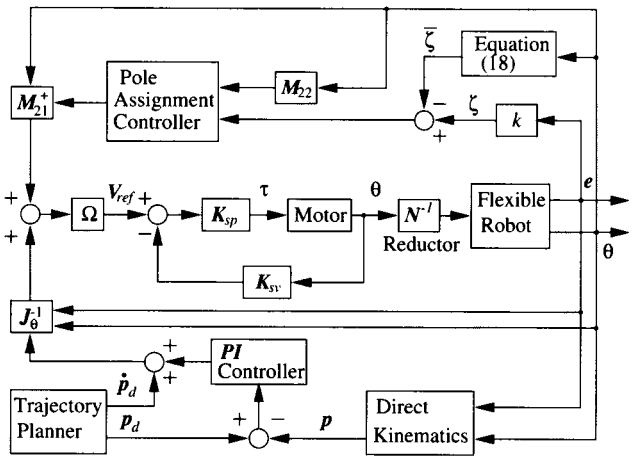

Fig. 4. A block diagram of the control system.

The sampling period T_s is set at 7.8125 [ms] (128 [Hz]). Based on extensive analyses,[26] the poles of closed-loop are chosen as

$$\Lambda_{1,2}=\begin{bmatrix} 0.826 & & & \mathbf{0} \\ & 0.826 & & \\ & & 0.913 & \\ \mathbf{0} & & & 0.913 \end{bmatrix} \pm \begin{bmatrix} 0.398 & & & \mathbf{0} \\ & 0.398 & & \\ & & 0.163 & \\ \mathbf{0} & & & 0.163 \end{bmatrix} j. \quad (53)$$

The gross motion control law Equation (13) in combination with vibration feedback control law Equation (47) is used to control the flexible manipulator to track a desired trajectory given in the Cartesian space in Equations (49) and (50).

Provided that the flexible manipulator does not work in the neighborhood of singularities, the Jacobian $\boldsymbol{J}_\theta$ is modeled in full as a nonlinear time-varying function in the experiment. Moreover, it is calculated and reversed at each sampling interval.

For FLEBOT II, after calculations the 4×4 spring constant matrix $\boldsymbol{K}_{22}(\boldsymbol{\theta})$ is given as

$$\boldsymbol{K}_{22}(\boldsymbol{\theta})=\begin{bmatrix} 1004 & -657 & 0 & 0 \\ 0 & 462 & 0 & 0 \\ 0 & 0 & 1004 & -657C_3 \\ 0 & 0 & 0 & 462 \end{bmatrix} \quad (54)$$

and $\widetilde{\boldsymbol{K}}_{22}(\boldsymbol{\theta})$ is as follows:

$$\widetilde{\boldsymbol{K}}_{22}(\boldsymbol{\theta})=\begin{bmatrix} 2.17 & -1.42 & 0 & 0 \\ 0 & 1 & 0 & 0 \\ 0 & 0 & 2.17 & -1.42C_3 \\ 0 & 0 & 0 & 1 \end{bmatrix} \quad (55)$$

Let $\boldsymbol{R}=\boldsymbol{M}_{21}^+\boldsymbol{M}_{22}$, with $n_f>n_r$. Therefore, $\boldsymbol{R}$ can be symbolically calculated as follows:

$$\boldsymbol{R}=\begin{bmatrix} 0 & 0 & R_{13} & R_{14} \\ 1/L_2 & 0 & 0 & 0 \\ 0.5/L_2 & (1-D_8)/L_3 & 0 & 0 \end{bmatrix} \quad (56)$$

where $S_2=\sin\theta_2$, $C_2=\cos\theta_2$, $S_3=\sin\theta_3$, $C_3=\cos\theta_3$, and $S_{23}=\sin(\theta_2+\theta_3)$, $C_{23}=\cos(\theta_2+\theta_3)$, and

$$\begin{aligned} R_{13} &= [m_3\sigma_1+(\sigma_1+\sigma_2)m_p(1+1.5L_3C_3/L_2)]/\sigma, \\ R_{14} &= (\sigma_1+\sigma_2)m_p(1-D_8C_3^2-D_9S_3^2)/\sigma, \\ \sigma_1 1 &= (m_3+m_p)L_2S_2+m_pL_3S_{23}, \\ \sigma_2 &= m_pL_2S_2+m_pL_3S_{23}, \\ \sigma &= \sigma_1^2+\sigma_2^2, \\ D_8 &= -3L_2E_3I_3/(4L_3E_2I_2), \\ D_9 &= -3L_2E_3I_3/(L_3G_2J_2). \end{aligned}$$

Therefore, in the case of FLEBOT II, $k=462$, and $\mu=0.00216$, as well as $\epsilon=\sqrt{\mu}=0.0465$.

If the same closed-loop poles of vertical deflections of last two links are selected, our method will become simple to implement. It is because that all coefficients for vertical vibration control become constant, only very few real-time calculations are involved in our method.

In trajectory tracking control, desired positions are time varying; the end-effector of FLEBOT II is driven to follow a spatial orbit given in Equation (50) twice.

First trial. Let the end-effector start to move from a starting point ($[54.2\ 55.6\ -6.5]^T$ [cm]) which is far from a zero-time point $\boldsymbol{p}=[59\ 50\ 0]^T$ [cm] on the desired trajectory in order to show the effectiveness of the proposed method in two respects. On the one hand, we are going to show the ability of the gross motion control Equation (13) to drive the end-effector to follow the desired trajectory well. On the other hand, we intended to show the capability of the vibration suppression control Equation (47) to damp out vibrations satisfactorily. Figures labeled from 5 to 14 represent the experimental results of first trial. It can be seen from Figures 9, 10, and 11 that the real trajectory approaches the desired trajectory approximately in about one second after the start.

Figures 5, 6, 7, and 8 demonstrate the time histories of vertical and horizontal deflections of the last two links in the first trial, respectively.

Figures 9, 10, and 11 illustrate the tracking trajectory on the x-axis, y-axis, and z-axis in the first trial, respectively.

Figures 12, 13, and 14 illustrate the tracking errors on the x-axis, y-axis, and z-axis in the first trial, respectively.

Second trial. Let the end-effector begin to move from the finish point of the first trial. Figures which span from 15 to

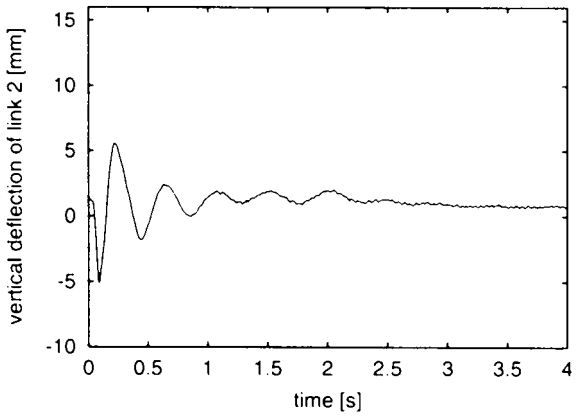

Fig. 5. Vertical deflection of link 2 in the first trial.

https://doi.org/10.1017/S0263574702004435 Published online by Cambridge University Press

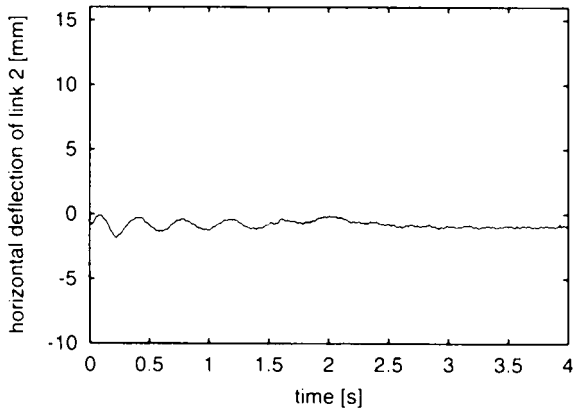

Fig. 6. Horizontal deflection of link 2 in the first trial.

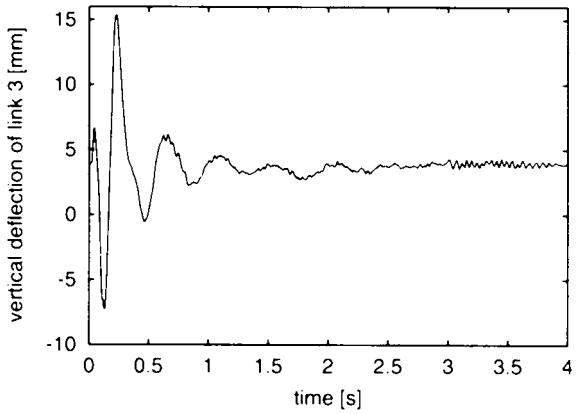

Fig. 7. Vertical deflection of link 3 in the first trial.

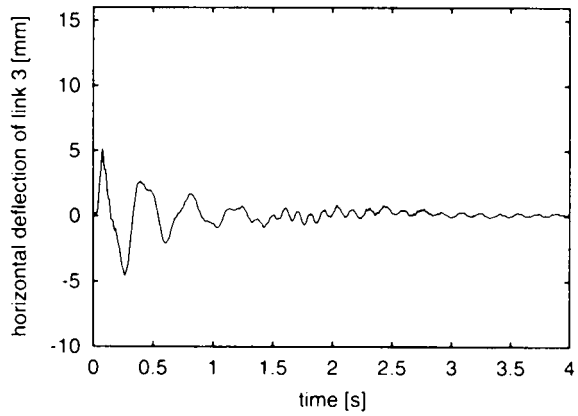

Fig. 8. Horizontal deflection of link 3 in the first trial.

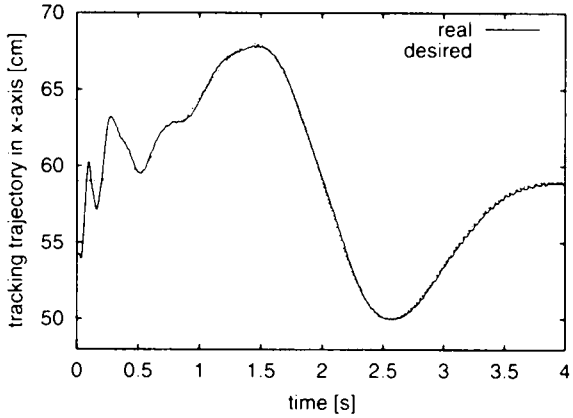

Fig. 9. Tracking trajectory in x-axis in the first trial.

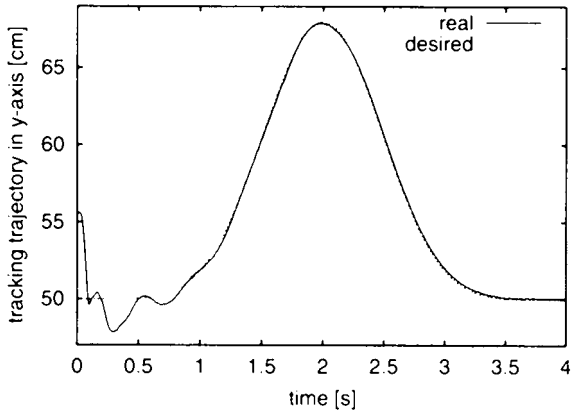

Fig. 10. Tracking trajectory in y-axis in the first trial.

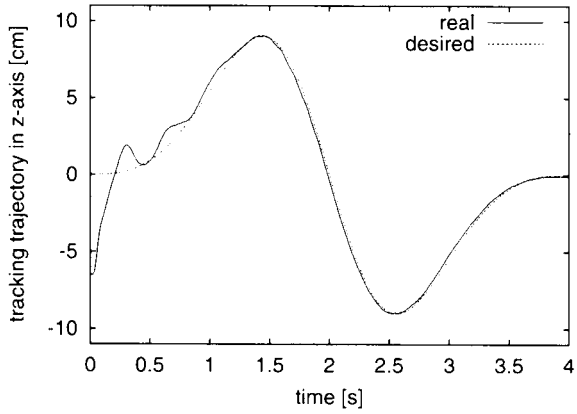

Fig. 11. Tracking trajectory in z-axis in the first trial.

30 indicate the experimental results of the second trial. It is observed that in the second trial the trajectory performance is improved a great deal due to minor deviations of starting point from zero-time point $\boldsymbol{p}=[59\ 50\ 0]^T$ [cm] on the desired trajectory. It is also noted that in the second trial magnitudes of vibrations are smaller than in the first trial, this is because vibrations are excited during initial tracking process when the end-effector approaches the desired trajectory rapidly after the start.

Figures 15, 16, 17, and 18 demonstrate the time histories of vertical and horizontal deflections of last two links in the second trial, respectively.

Figures 19, 20, and 21 illustrate the tracking trajectory on the x-axis, y-axis, and z-axis in the second trial, respectively.

Figures 22, 23, and 24 illustrate the tracking errors on the x-axis, y-axis, and z-axis in the second trial, respectively.

Figures 25, 26, and 27 illustrate the real accelerations in joints 1, 2, and 3 in the second trial, respectively.

Figure 28 shows the trace of end-effector in x-y plane with vibration control in the second trial. The projection of trajectory in the x-y plane is used to draw the trace of the end-effector.

Figure 29 shows the trace of end-effector in the x-z plane with vibration control in the second trial. The projection of

https://doi.org/10.1017/S0263574702004435 Published online by Cambridge University Press

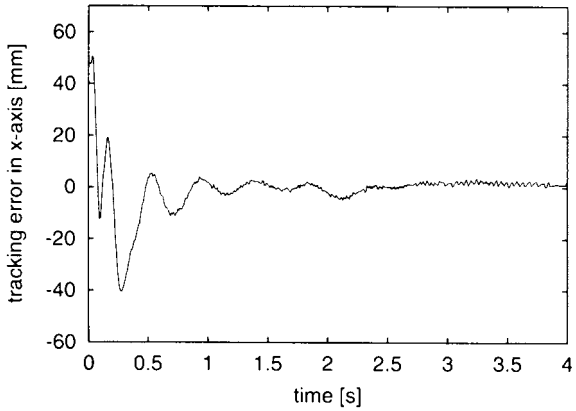

Fig. 12. Tracking errors in x-axis in the first trial.

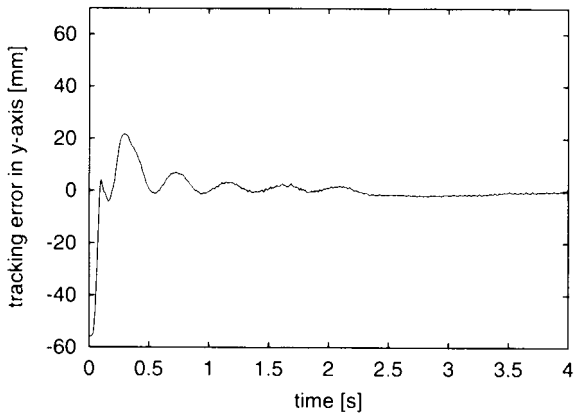

Fig. 13. Tracking errors in y-axis in the first trial.

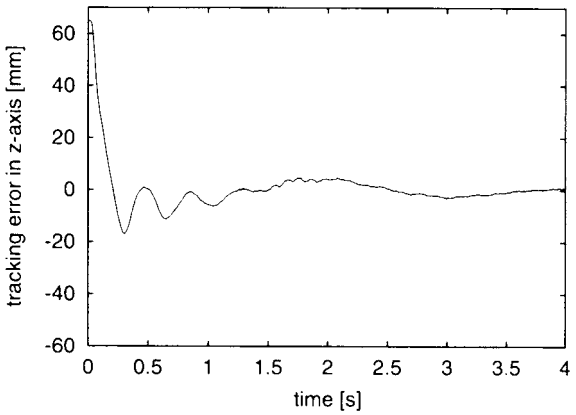

Fig. 14. Tracking errors in z-axis in the first trial.

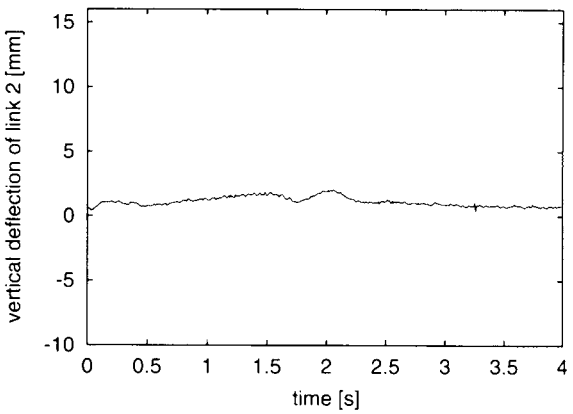

Fig. 15. Vertical deflection of link 2 in the second trial.

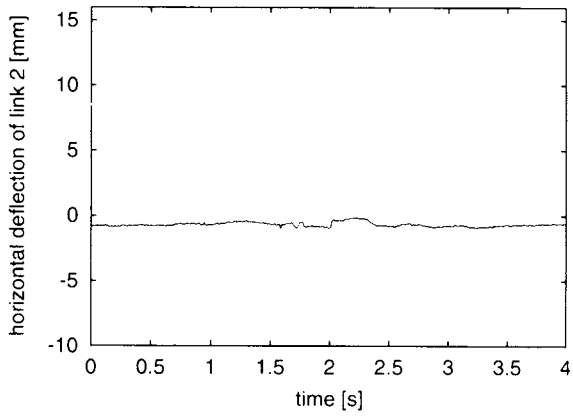

Fig. 16. Horizontal deflection of link 2 in the second trial.

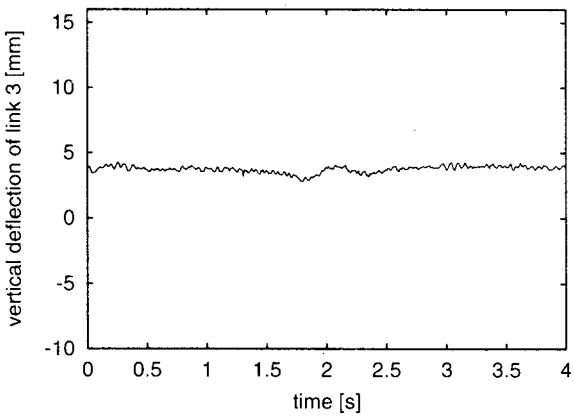

Fig. 17. Vertical deflection of link 3 in the second trial.

trajectory on the x-z plane is used to draw the trace of the end-effector.

Figure 30 shows the trace of end-effector in the y-z plane with vibration control in the second trial. The projection of trajectory on the y-z plane is used to draw the trace of the end-effector.

In those figures, Figures 9, 10, 11 in the first trial, and Figures 19, 20, 21, and from 25 to 30 in the second trial, the real line represents the real values gained from experiments and the line with dot marks represents the values calculated from the desired trajectory.

As can be concluded from the experimental results, the tracking errors which occur at the end of trajectory in the first trial are $[2.2 \ \ -0.5 \ \ 0.9]^T$ [mm], in the second trial are $[-0.6 \ \ 0.5 \ \ 0.6]^T$ [mm] this shows that the control strategy described in this paper is not only able to damp out vibrations, but also able to obtain satisfactorily final positioning.

It has been found that when joint accelerations change precipitously, bigger trajectory tracking errors are more likely to occur. During the experiments, it was observed that the performance of the control system degraded as the duration of motion was decreased. If the value of T is below

https://doi.org/10.1017/S0263574702004435 Published online by Cambridge University Press

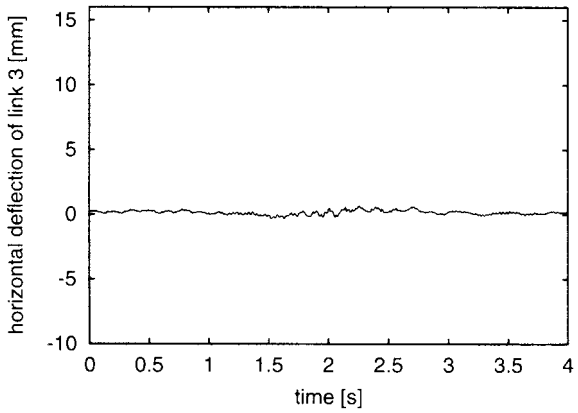

Fig. 18. Horizontal deflection of link 3 in the second trial.

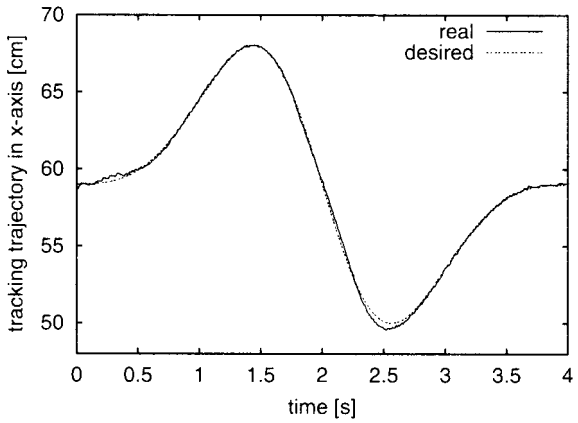

Fig. 19. Tracking trajectory in x-axis in the second trial.

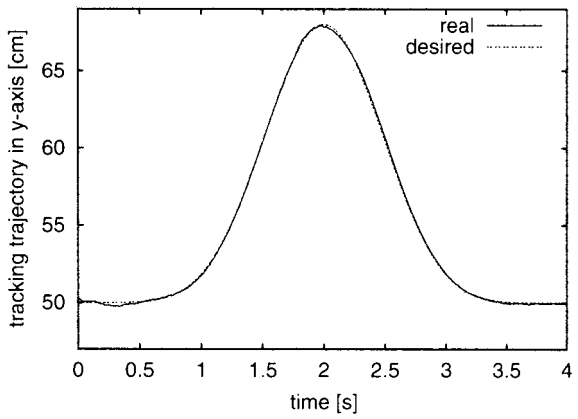

Fig. 20. Tracking trajectory in y-axis in the second trial.

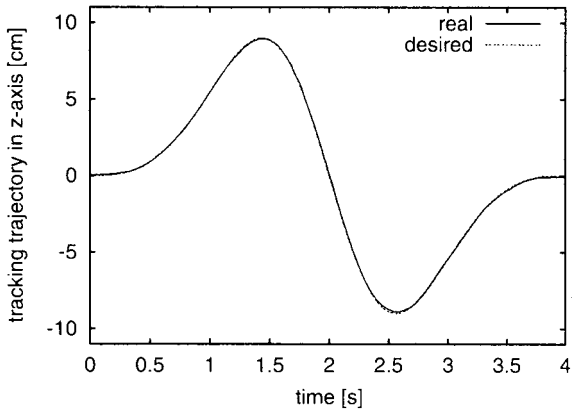

Fig. 21. Tracking trajectory in z-axis in the second trial.

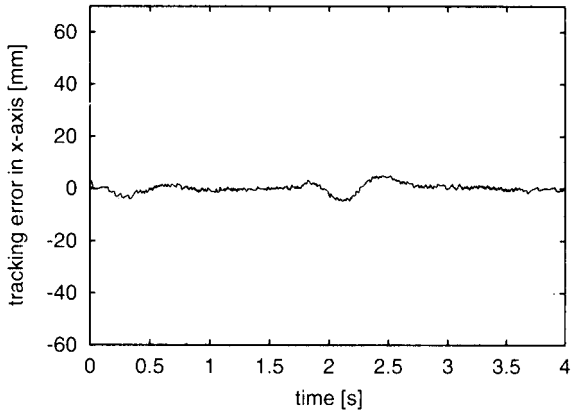

Fig. 22. Tracking errors in x-axis in the second trial.

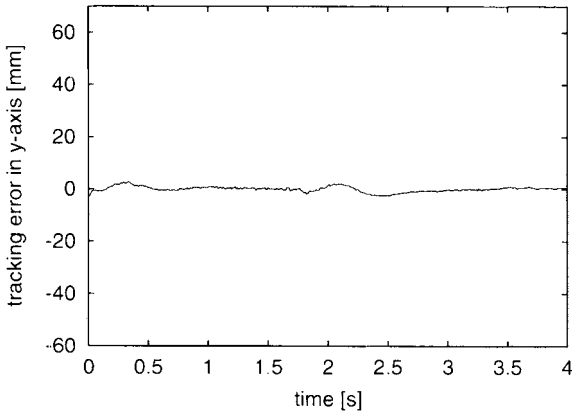

Fig. 23. Tracking errors in y-axis in the second trial.

the lower allowable limit, say 2 [s], the tracking errors became no longer tolerable.

7. DISCUSSION

Notice that in our approach we assume that the flexible manipulator knows the weight of the payloads that it is carrying; unquestionably, the vibration damping method proposed in this paper may be inadequate because it neglects the changes of the load in a task cycle. These changes in the payload of the controlled flexible subsystem are significant enough to render vibration feedback control ineffective. In order to overcome this drawback, an adaptive control method should be introduced to estimate the parameters on-line and compensate for load changes during a task cycle.

It goes without saying that the dynamics of flexible manipulators including an inverse dynamics computation, and the dynamic modeling is the first step for the design of control systems for flexible manipulators. The two main

https://doi.org/10.1017/S0263574702004435 Published online by Cambridge University Press

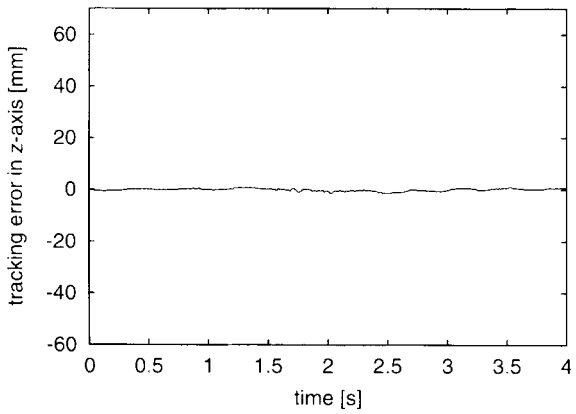

Fig. 24. Tracking errors in z-axis in the second trial.

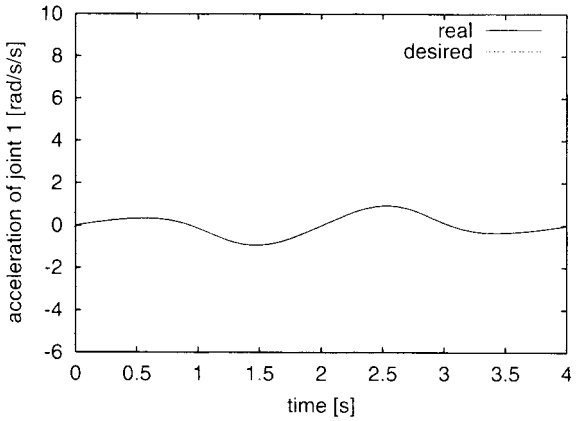

Fig. 25. Acceleration of joint 1 in the second trial.

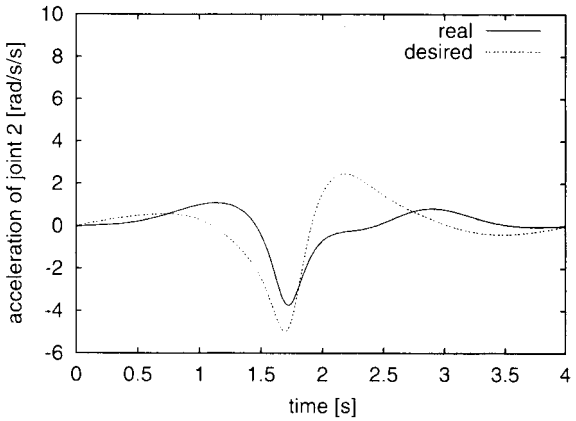

Fig. 26. Acceleration of joint 2 in the second trial.

approaches to the flexible manipulator dynamics have been the finite element method[38] and the assumed rmodes method.[39] However, in our paper, the lumped-parameter approach is used in the design and analysis of a flexible subsystem. This model has been successfully used in vibration suppression control[4, 26, 27] and controllability analysis.[37]

An evident advantage of our approach is that it does not require a derivative of strain gauge signals for the vibration suppression, since determining the values of velocities ($\dot{\boldsymbol{e}}$) by differentiation of deflections ($\boldsymbol{e}$) may result in values that

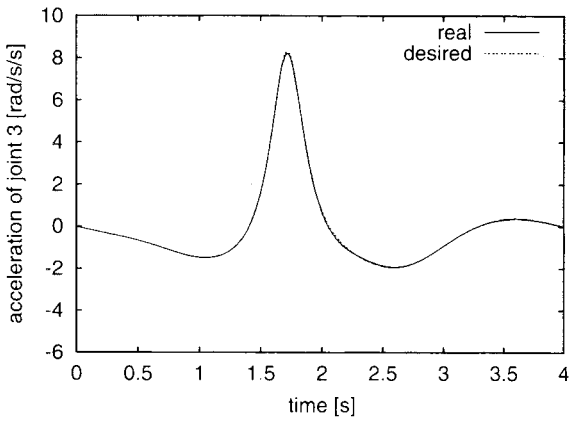

Fig. 27. Acceleration of joint 3 in the second trial.

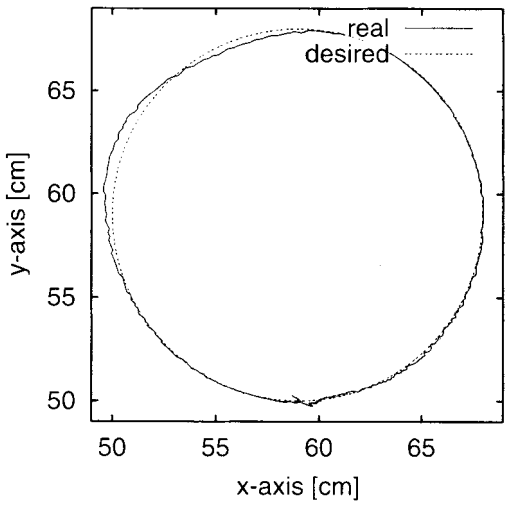

Fig. 28. Trace of end-effector in the x-y plane with vibration control in the second trial.

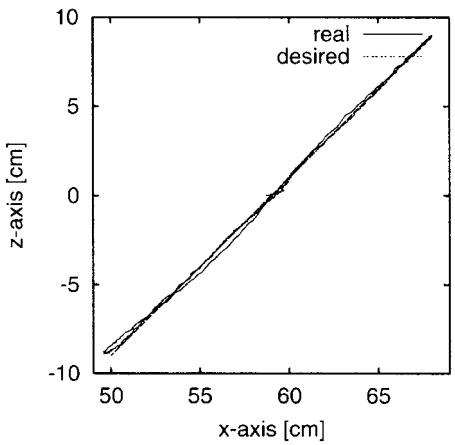

Fig. 29. Trace of end-effector in the x-z plane with vibration control in the second trial.

contain a subtantial amount of noise. The control scheme proposed requires measurements of deflections ($\boldsymbol{e}$) The strain gauge located at the roots of the rods are used for measuring the elements of ($\boldsymbol{e}$) but in doing so, one will have to contend with the possibility of the problem of non-colocation of actuators and sensors reappearing. In order to

https://doi.org/10.1017/S0263574702004435 Published online by Cambridge University Press

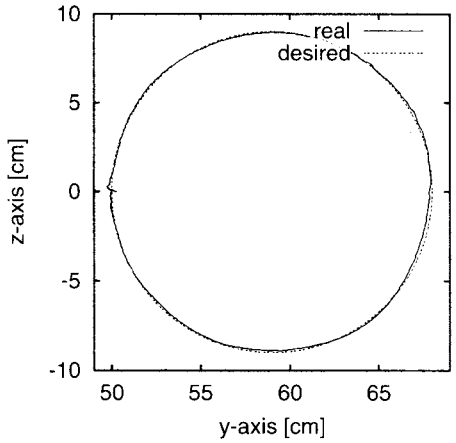

Fig. 30. Trace of end-effector in the *y*-*z* plane with vibration control in the second trial.

overcome the problem of noncolocation, we attach strain gauges to the points which are very near to the actuators. Also, the high frequency modes are filtered out by an appropriately designed low-pass filter.

It is noteworthy that a PI method has been proposed based upon the Cartesian space errors at the end-effector during the trajectory tracking. Therefore, the embarassing inverse kinematic solution is avoided, which makes the proposed method easier to employ in real implementation.

It should be mentioned that since the Jacobian matrix in our approach is used, a question arises as to the invertibility of the Jacobian matrix (i.e. avoidance of singularities). The assumption that $\boldsymbol{J}_\theta$ must be invertible limits the moving space of flexible manipulator significantly.

Last but not the least, it should be pointed out that the above discussions are based on the assumption that the control motor drivers are of a speed reference type, hence in such a case, Equation (11) can be reduced into Equation (12). However, it is worth noting that if the motor drivers are of a torque control type, and if the flexible manipulator moves at exceedingly high speeds or joint accelerations are extremely large, then theoretically and practically the control law proposed is no longer effective.

8. CONCLUSIONS

A singularly perturbed method of a Cartesian-based PI control of a three-link, spatial flexible manipulator has been described in this paper. Our main emphasis has been on designing a composite controller for achieving accurate end-effector positioning and trajectory tracking of a predetermined trajectory, and for stabilizing the flexible subsystem. For the flexible subsystem, a pole assignment control along the motion equilibrium trajectory under the gross motion control is headed. Experiments on the trajectory tracking control were conducted. These experimental results demonstrate that a pole assignment feedback control can damp out vibrations satisfactorily, and the gross motion PI control is able to maintain good performance in the motion of a flexible manipulator. This is very important in practice, since it would be senseless if the vibration suppression were obtained at the cost of seriously deteriorating the tracking performance of motion of a flexible manipulator. The ultimate control goal of flexible robots is simultaneous motion/vibration control and not vibration suppression only. Practical concerns for implementation this strategy are discussed both advantageously and disavantageously.

Acknowledgements

The authors gratefully acknowledge the cooperation of this work with the colleagues in the Spacecraft Systems Laboratory of the Department of Aeronautics and Space Engineering at Tohoku University. The first author would like to express his thanks to Japanese Education Ministry for supplying a scholarship to him during his stay in Japan.

References

1. W. J. Book, O. Maizza-Neto and D. Z. Whitney, "Feedback Control of Two Beam, Two Joint Systems with Distributed Flexibility", *ASME J. of Dynamic Systems, Measurement, and Control* **87**(4), 424–431 (1975).
2. R. H. Cannon Jr. and E. Schmitz, "Initial Experiments on the End-point Control of a Flexible One-link Robot", *Int. J. Robotics Research* **3**(3), 62–75 (1984).
3. J. Yuh, "Application of Discrete Time Model Reference Adaptive Control to a Flexible Single Link Robot", *Int. J. Robotics Research* **4**(5), 621–630 (1987).
4. M. Uchiyama and A. Konno, "Computed Acceleration Control for the Vibration Suppression of Flexible Robotic Manipulators", *Proc. 5th Int. Conf. on Advanced Robotics* (l991) pp. l26–131.
5. T. D. Looke, M. Farooq and M. M. Bayoumi, "The Response of a One Link, Flexible Arm to Variable Structure Control Using Sliding Surfaces", *Proc. 5th IFAC Symposium of Control DPS* (1989) pp. 237–241.
6. J. Bontseme, R. F. Curtain and J. M. Schumacher, "Robust Control of Flexible Systems: A Case Study", *Automatica* **24**, 177–186 (1988).
7. N. C. Singer and W. P. Seering, "Using Acausal Shaping Techniques to Reduce Robot Vibration", *Proc. IEEE Int. Conf. on Robotics and Automation*, Philadelphia (1989) pp. 888–893.
8. N. C. Singer and W. P. Seering, "Preshaping Commands Inputs to Reduce System Vibration", *ASME J. of Dynamic Systems, Measurement, and Control* **112**(1), 76–82 (1990).
9. J. M. Hyde and W. P. Seering, "Using Input Command Preshaping to Suppress Multiple Mode Vibration", *Proc. IEEE Int. Conf. on Robotics and Automation*, Sacramento, California (1991) pp. 2604–2609.
10. L. C. Lin and T. W. Yih, "Rigid Model-Based Neural Network Control of Flexible-link Manipulators", *Transactions ofIEEE on Robotics and Automation* **12**(4), 595–602 (1996).
11. B. Gebler, "Feed-Forward Control Strategy for an Industrial Robot with Elastic Arms", *Proc. of IEEE Int. Conf. on Robotics and Automation* (1987) pp. 923–928.
12. G. D. Maria and B. Siciliano, "A Multi-Layer Approach to Control of a Flexible Arm", *Proc. of IEEE Int Conf. on Robotics and Automation* (1987) 774–778.
13. B. Siciliano and W. Book, "A Singular Perturbation Approach to Control of Lightweight Flexible Manipulators", *Int. J. Robotics Research* **7**(4), 79–90 (1988).
14. F. L. Lewis and M. Vandegrift, "Flexible Robot Arm Control by a Feedback Linearization/Singular Perturbation Approach", *Proc. of IEEE Int. Conf. on Robotics and Automation* (1993) pp. 729–734.
15. W. Yim, "End-Point Trajectory Control, Stabilization, and Zero Dynamics of a Three-Link Flexible Manipulator", *Proc. of IEEE Int Conf. on Robotics and Automation* (1993) pp. 468–473.

https://doi.org/10.1017/S0263574702004435 Published online by Cambridge University Press

16. Z. H. Luo, N. Kitamura, and B. Z. Guo, "Shear Force Feedback Control of Flexible Robot Arms", *Transactions of IEEE on Robotics and Automation* **11**(5), 760-765 (1995).
17. C. Damaren, "Modal Properties and Control System Design for Two-Link Flexible Manipulators", *Int. J. Robotics Research* **17**(6), 667–678 (1998).
18. F. Xi and R. G. Fenton, "Point-to-point Quasi-static Motion Planning for Flexible-link Manipulators", *Transaction of IEEE on Robotics and Automation* **11**(5), 770–776 (1995).
19. Y. Q. Dai, A. A. Loukianov and M. Uchiyama, "A Hybrid Numerical Method for Solving the Inverse Kinematics of a Class of Flexible Manipulators", *Proc. of IEEE Int Conf. on Robotics and Automation*, New Mexico, USA (1997) pp. 3449–3454.
20. M. Uchiyama, Z. H. Jiang and K. Hakomori, "Compensating Control of a Flexible Robot Arm", *J. of Robotics and Mechatronics* **2**(2), 97–106 (1990).
21. M. Uchiyama and Z. H. Jiang, "Compensability of End-Effector Position Error for Flexible Robot Manipulator", *Proc. of American Control Conference* (1991) pp. 1873–1878.
22. F. Pfeiffer and B. Gebler, "A Multi-Stage Approach to the Dynamics and Control of Elastic Robots", *Proc. of IEEE Int. Conf. on Robotics and Automation* (1988) pp. 2–8.
23. J. O. King, V. G. Gourishankar and R. Z. Rink, "Composite Pseudolink End-point Control of Flexible Manipulators", *IEEE Transactions on Systems, Man, and Cybernetics* **20**(5), 967–977 (1990).
24. M. W. Spong, K. Khorasani and P. V. Kokotovic, "An Integral Manifold Approach to the Feedback Control of Flexible Joint Robots", *Transactions of IEEE on Robotics and Automation* **3**(4), 291–299 (1987).
25. D. F. Golla, S. C. Garg and P. C. Hughes, "Linear State-Feedback Control of Manipulators", *Mech. Machine Theory* **16**, 93–103 (1981).
26. S. López-Linares, A. Konno and M. Uchiyama, "Vibration Suppression Control of 3D Flexible Robots Using Velocity Inputs", *J. of Robotic Systems* **14**(12), 823–837 (1997).
27. A. Konno and M. Uchiyama, "Vibration Suppression Control of Spatial Flexible Manipulators", *IFAC Control Engineering Practice* **3**(9), 1315–1321 (1995).
28. E. Bayo, M. A. Serna, P. Papadopoulos and J. Stubbe, "Inverse Dynamics of Multi-link Elastic Robot: An Iterative Frequency Domain Approach", *Int. J. Robotics Research* **8**(6), 49–62 (1989).
29. F. Pfeiffer, "A Feedforward Decoupling Concept for the Control of Elastic Robots", *J. of Robotic Systems* **6**(4), 407–416 (1989). 30. D. M. Gorinevsky, A. V. Lensky and E. I. Sabitov, "Feedback Control of One-Link Flexible Manipulator with Gear Train", *J. of Robotic Systems* **8**(5), 659–676 (1991).
31. W. J. Book, H. Lane, L. J. Love, D. P. Magee and K. Obergfell, "A Novel Teleoperated Long-Reach Manipulator Testbed and its Remote Capabilities via the Internet", *Proc. of IEEE Int. Conf. on Robotics and Automation* (1996) pp. l036–1041.
32. R. Marino and S. Nicosia, "Singular Perturbation Techniques in the Adaptive Control of Elastic Robots", *1st IFAC Symposium on Robot Control* (1985) pp. 95–100.
33. P. V. Kokovic, "Applications of Singular Perturbation Techniques to Control Problems", *SIAM Review* **26**(4), 501–550 (1984).
34. K. Khorasani and M. W. Spong, "Invariant Manifolds and Their Application to Robot Manipulators with Flexible Joints", *Proc. of IEEE Int. Conf. on Robotics and Automation* (l985) pp. 978–983.
35. R. J. Theodore and A. Ghosal, "Comparison of the Assessment Modes and Finite Element Models for Flexible Multilink Manipulators", *Int. J. Robotics Research* **4**(2), 91–111 (1995).
36. L. A. Nguyen, I. D. Walker and R. J. P. DeFigueiredo, "Dynamic Control of Flexible, Kinematically Redundant Robot Manipulators", *Transactions of IEEE on Robotics and Automation* **8**(6), 759–767 (1992).
37. A. Konno, M. Uchiyama, Y. Kito and M. Murakami, "Configuration-Dependent Vibration Controllability of Flexible-Link Manipulators", *Int. J. Robotics Research* **16**(4), 567–576 (1997).
38. P. B. Usoro, R. Nadira and S. S. Mahil, "A Finite Element/Lagrange Approach to Modeling Lightweight Flexible Manipulators", *ASME J. of Dynamic Systems, Measurement, and Control* **108**(1), 198–205 (1986).
39. W. J. Book, "Recursive Langrangian Dynamics of Flexible Manipulator Arms", *Int. J. Robotics Research* **3**(3), 87–101 (1984).

APPENDIX

A part of the kinematic and dynamic model of three-link, spatial flexible manipulator, FLEBOT II, in the Sapcecraft Systems Laboratory of the Department of Aeronautics and Space Engineering at Tohoku University is presented as:

$$\boldsymbol{p}=[p_x \;\; p_y \;\; p_z]^T$$

and

$$\begin{aligned}
p_x &= L_2 C_2 + L_3 C_{23} - \boldsymbol{e}_{y2} S_2 - \boldsymbol{e}_{y3} S_{23} - L_3 S_{23} \phi_{z2}, \\
p_y &= C_1[L_2 S_2 + L_3 S_{23} + L_3 C_{23} \phi_{z2} + \boldsymbol{e}_{y2} C_2 + \boldsymbol{e}_{y3} C_{23}] \\
&\quad - S_1[-L_3 C_3 \phi_{y2} + L_3 S_3 \phi_{x2} + \boldsymbol{e}_{z2} + \boldsymbol{e}_{z3}], \\
p_z &= S_1[L_2 S_2 + L_3 S_{23} + L_3 C_{23} \phi_{z2} + \boldsymbol{e}_{y2} C_2 + \boldsymbol{e}_{y3} C_{23}] \\
&\quad + C_1[-L_3 C_3 \phi_{y2} + L_3 S_3 \phi_{x2} + \boldsymbol{e}_{z2} + \boldsymbol{e}_{z3}]
\end{aligned}$$

and the rigid Jacobian matrix is

$$\boldsymbol{J}_\theta = \begin{bmatrix} J_{\theta 11} & J_{\theta 12} & J_{\theta 13} \\ J_{\theta 21} & J_{\theta 22} & J_{\theta 23} \\ J_{\theta 31} & J_{\theta 32} & J_{\theta 33} \end{bmatrix}$$

where

$$\begin{aligned}
J_{\theta 11} &= 0, \\
J_{\theta 12} &= -L_2 S_2 - L_3 S_{23} - \boldsymbol{e}_{y2} C_2 - \boldsymbol{e}_{y3} C_{23} - L_3 C_{23} \phi_{z2}, \\
J_{\theta 13} &= -L_3 S_{23} - \boldsymbol{e}_{y3} C_{23} - L_3 C_{23} \phi_{z2}, \\
J_{\theta 21} &= -S_1[L_2 S_2 + L_3 S_{23} + L_3 C_{23} \phi_{z2} + \boldsymbol{e}_{y2} C_2 \\
&\quad + \boldsymbol{e}_{y3} C_{23}] - C_1[-L_3 C_3 \phi_{y2} + L_3 S_3 \phi_{x2} + \boldsymbol{e}_{z2} + \boldsymbol{e}_{z3}], \\
J_{\theta 22} &= C_1[L_2 C_2 + L_3 C_{23} - L_3 S_{23} \phi_{z2} - \boldsymbol{e}_{y2} S_2 - \boldsymbol{e}_{y3} S_{23}], \\
J_{\theta 23} &= C_1[L_3 C_{23} - L_3 S_{23} \phi_{z2} - \boldsymbol{e}_{y3} S_{23}] \\
&\quad - S_1[L_3 S_3 D_{10} \boldsymbol{e}_{z2} + 2 S_3 C_3 D_8 \boldsymbol{e}_{z3} - 2 S_3 C_3 D_9 \boldsymbol{e}_{z3}], \\
J_{\theta 31} &= C_1[L_2 S_2 + L_3 S_{23} + L_3 C_{23} \phi_{z2} + \boldsymbol{e}_{y2} C_2 + \boldsymbol{e}_{y3} C_{23}] \\
&\quad - S_1[-L_3 C_3 \phi_{y2} + L_3 S_3 \phi_{x2} + \boldsymbol{e}_{z2} + \boldsymbol{e}_{z3}], \\
J_{\theta 32} &= S_1[L_2 C_2 + L_3 C_{23} - L_3 S_{23} \phi_{z2} - \boldsymbol{e}_{y2} S_2 - \boldsymbol{e}_{y3} S_{23}], \\
J_{\theta 33} &= S_1[L_3 C_{23} - L_3 S_{23} \phi_{z2} - \boldsymbol{e}_{y3} S_{23}] \\
&\quad + C_1[L_3 S_3 D_{10} \boldsymbol{e}_{z2} + 2 S_3 C_3 D_8 \boldsymbol{e}_{z3} - 2 S_3 C_3 D_9 \boldsymbol{e}_{z3}].
\end{aligned}$$

The joint variable vector $\boldsymbol{\theta}$ and deflection variable vector $\boldsymbol{e}$ are defined as

$$\begin{aligned}
\boldsymbol{\theta} &= [\theta_1 \;\; \theta_2 \;\; \theta_3]^T, \\
\boldsymbol{e} &= [e_1 \;\; e_2 \;\; e_3 \;\; e_4]^T = [e_{y2} \;\; e_{y3} \;\; e_{z2} \;\; e_{z3}]^T
\end{aligned}$$

and the flexible Jacobian matrix is

https://doi.org/10.1017/S0263574702004435 Published online by Cambridge University Press

$$\boldsymbol{J}_e = \begin{bmatrix} J_{e11} & J_{e12} & J_{e13} & J_{e14} \\ J_{e21} & J_{e22} & J_{e23} & J_{e24} \\ J_{e31} & J_{e32} & J_{e33} & J_{e34} \end{bmatrix}$$

where

$$\begin{aligned}
J_{e11} &= -S_2 + L_3 S_{23} D_{10}, \\
J_{e12} &= -S_{23}(1 - D_8), \\
J_{e13} &= 0, \\
J_{e14} &= 0, \\
J_{e21} &= C_1(C_2 - L_3 C_{23} D_{10}), \\
J_{e22} &= C_1 C_{23}(1 - D_8), \\
J_{e23} &= -S_1(1 - L_3 C_3 D_{10}), \\
J_{e24} &= -S_1(1 - C_3^2 D_8 - S_3^2 D_9), \\
J_{e31} &= S_1(C_2 - L_3 D_{23} D_{10}), \\
J_{e32} &= S_1 C_{23}(1 - D_8), \\
J_{e33} &= C_1(1 - L_3 C_3 D_{10}), \\
J_{e34} &= C_1(1 - C_3^2 D_8 - S_3^2 D_9).
\end{aligned}$$

Inertia matrices and stiffness matrix as well as gravity vectors are given as follows:

$$\boldsymbol{M}_{11} = \begin{bmatrix} I_{m1} + m_3 L_2^2 S_2^2 + m_p D_1^2 + m_p L_3^2 D_3^2 & -m_p L_3 D_2 D_3 & m_p L_3 D_5 \\ -m_p L_3 D_2 D_3 & I_{m2} + m_3 L_2^2 + m_p (L_2 + L_3 C_{3\phi})^2 + m_p L_3^2 S_{3\phi}^2 & m_p L_3 (L_2 C_{3\phi} + L_3) \\ m_p L_3 D_5 & m_p L_3 (L_2 C_{3\phi} + L_3) & I_{m3} + m_p L_3^2 (1 + D_4^2 + \phi_{z2}^2) \end{bmatrix},$$

$$\boldsymbol{M}_{12} = \begin{bmatrix} m_p L_3 D_3 (C_2 + D_{10} L_3 C_{23}) & -m_p L_3 C_{23} D_3 (1 + D_8) \\ m_3 L_2 + m_p L_3 (D_6 + D_7) & m_p (L_2 C_2 + L_3)(1 + D_8) \\ m_p L_3 D_7 & m_p L_3 (1 + D_8) \end{bmatrix}$$

$$\begin{bmatrix} m_3 L_2 S_2 + m_p D_1 D_6 & m_p D_1 (1 - D_8 C_3^2 - D_9 S_3^2) \\ 0 & 0 \\ m_p L_3 D_4 D_6 & m_p L_3 D_4 (1 - D_8 C_3^2 - D_9 S_3^2) \end{bmatrix},$$

$$M_{12} = M_{21}^T$$

$$\boldsymbol{M}_{22} \begin{bmatrix} m_3 + m_p D_6 & m_p C_3 (1 - D_8) \\ m_p (C_3 - D_{10}) & m_p (1 - D_8) \\ 0 & 0 \\ 0 & 0 \end{bmatrix}$$

$$\begin{bmatrix} 0 & 0 \\ 0 & 0 \\ m_3 + m_p D_6 & m_p (1 - D_8 C_3^2 - D_9 S_3^2) \\ m_p D_6 & m_p (1 - D_8 C_3^2 - D_9 S_3^2) \end{bmatrix},$$

$$\boldsymbol{K}_{22} \begin{bmatrix} D_{11} & L_3 D_{10} D_{12} & 0 & 0 \\ 0 & D_{12} & 0 & 0 \\ 0 & 0 & D_{11} & L_3 C_3 D_{10} D_{12} \\ 0 & 0 & 0 & D_{12} \end{bmatrix},$$

$$\boldsymbol{g}_1 = \begin{bmatrix} 0 \\ (m_3 L_2 S_2 + m_p D_1) g \\ m_p L_3 (S_{23} + C_{23} \phi_{z2}) g \end{bmatrix},$$

$$\boldsymbol{g}_2 = \begin{bmatrix} (m_3 + m_p) S_2 g \\ m_p S_{23} g \\ 0 \\ 0 \end{bmatrix}$$

where g is the gravity coefficient and equals approximately 9.8062 [m/s^2].

$$\begin{aligned}
C_{3\phi} &= C_3 - \phi_{z2} S_3, \\
S_{3\phi} &= S_3 + \phi_{z2} C_3, \\
D_1 &= L_2 S_2 + L_3 S_{23} + L_3 \phi_{z2} C_{23}, \\
D_2 &= L_2 C_2 + L_3 C_{23} - L_3 \phi_{z2} S_{23}, \\
D_3 &= S_3 \phi_{x2} - C_3 \phi_{y2}, \\
D_4 &= C_3 \phi_{x2} + S_3 \phi_{y2}, \\
D_5 &= L_2 S_2 (C_3 \phi_{x2} + S_3 \phi_{y2}) + L_3 (S_2 \phi_{x2} + C_2 \phi_{y2}) \\
&\quad + L_2 \phi_{z2} (C_2 \phi_{x2} - S_2 \phi_{y2}), \\
D_6 &= 1 - \frac{K_{e2}}{K_{d2}} L_3 C_3, \\
D_7 &= C_{3\phi} - L_3 \frac{K_{e2}}{K_{d2}}, \\
D_8 &= \frac{L_3^2}{K_{d2}} \left(\frac{K_{e3}^2}{K_{d3}} - K_{b3} \right), \\
D_9 &= \frac{L_3^2}{K_{c2}} \left(\frac{K_{e3}^2}{K_{d3}} - K_{b3} \right), \\
D_{10} &= \frac{K_{e2}}{K_{d2}}, \\
D_{11} &= K_{b2} - \frac{K_{e2}^2}{K_{d2}}, \\
D_{12} &= K_{b3} - \frac{K_{e3}^2}{K_{d3}}, \\
\phi_{x2} &= -\frac{L_3 S_3}{K_{c2}} \left(\frac{K_{e3}^2}{K_{d3}} - K_{b3} \right) \boldsymbol{e}_{z3},
\end{aligned}$$

https://doi.org/10.1017/S0263574702004435 Published online by Cambridge University Press

$$\phi_{y2}=\frac{K_{e2}}{K_{d2}}\boldsymbol{e}_{z2}+\frac{L_3C_3}{K_{d2}}\left(\frac{K_{e3}^2}{K_{d3}}-K_{b3}\right)\boldsymbol{e}_{z3},$$

$$\phi_{z2}=-\frac{K_{e2}}{K_{d2}}\boldsymbol{e}_{y2}-\frac{L_3}{K_{d2}}\left(\frac{K_{e3}^2}{K_{d3}}-K_{b3}\right)\boldsymbol{e}_{y3},$$

$$\phi_{x3}=0,$$

$$\phi_{y3}=\frac{K_{e3}}{K_{d3}}\boldsymbol{e}_{z3},$$

$$\phi_{z3}=-\frac{K_{e3}}{K_{d3}}\boldsymbol{e}_{y3},$$

$$K_{bi}=\frac{12E_iI_i}{L_i^3},\quad i=2,3,$$

$$K_{ci}=\frac{G_iJ_i}{L_i},$$

$$K_{di}=\frac{4E_iI_i}{L_i},$$

$$K_{ei}=-\frac{6E_iI_i}{L_i^2}.$$

where ϕ_{x2}, ϕ_{y2}, ϕ_{z2}, ϕ_{x3}, ϕ_{y3}, ϕ_{z3} are deflectional angles. For the other terms in the kinematic and dynamic equations of FLEBOT II, the interested reader is referred to reference 26.

https://doi.org/10.1017/S0263574702004435 Published online by Cambridge University Press